Current Research in Food Science 10 (2025) 100948

Contents lists available at ScienceDirect

Current Research in Food Science

journal homepage: www.sciencedirect.com/journal/current-research-in-food-science

Design and test of steam-injected continuous scrambled egg device

Liangyu Xue [a,b], Xiaojia Hu [a], Bo Qi [c], Yibing Yuan [c], Wensong Wei [a,b,*], Ping Yang [a], Xin Ai [a], Fangting Fu [b], Chunhui Zhang [a,b,**]

[a] Institute of Food Science and Technology, Chinese Academy of Agricultural Sciences/Key Laboratory of Agricultural Product Processing, Ministry of Agriculture, Beijing, 100193, China
[b] Zibo Institute for Digital Agriculture and Rural Research, Zibo, 255051, China
[c] Beijing Key Laboratory of Sensors, Beijing Information Science and Technology University, Beijing, 100101, China

ARTICLE INFO

Keywords:
Agricultural machinery
Steam device
Industrially manufactured
Continuous culinary
Performance verification

ABSTRACT

To solve the existing problems of low yield, uneven quality, and single form of industrially scrambled eggs, we have developed a continuous high-output steam scrambled egg device based on the principle of steam injected. By establishing calibration curves for egg, oil, and steam flow rates, determining the key parameters of the equipment, and simulating the heat transfer process between steam and egg by Computational Fluid Dynamics (CFD), we created the device and verified its production performance. The results show that the capacity of this device can reach 104.4 kg/h, which greatly improves production efficiency. By precisely adjusting the steam flow, this device can produce scrambled eggs in the form of blocks, thick slices, thin slices, and broken. Moreover, the differences between the scrambled eggs produced by this device and the traditional frying pan were not significant in terms of color, taste and sensory evaluation ($p > 0.05$). Most importantly, this device produces scrambled eggs with better elasticity, softer texture, and better overall uniformity of maturity to achieve consumer satisfaction. This study provides technical support for the industrialized continuous production of Chinese egg dishes.

1. Introduction

Eggs are one of the most common culinary foods due to their rich nutrient profile (Sâmia et al., 2022). Scrambled eggs are a very ancient and common household dish that can be dated back thousands of years. Scrambled eggs (especially with a little butter) became a common dish to cook in Europe. In Asia, scrambled eggs play an important role in Chinese (e.g. scrambled eggs with tomatoes) and Japanese (e.g. tamagoyaki) cuisine. With the development of the Internet and the extensive use of social media, Chinese cuisine is increasingly popular. Scrambled eggs are often mixed with others, such as rice, tomatoes, and cucumbers, to become one of the essential stir-fry ingredients. The different form of scrambled eggs in these dishes further drives the demand for multi-form scrambled eggs in industrialized dishes.

At present, a planetary interlayer boiler or roller-frying pan is mainly used to produce Chinese culinary dishes. Chapin Roger invented a dish-cooking robot that can precisely adjust the temperature, stirring speed, and time during dish cuisine (Chapin, 1983). In the continuous thermal processing device, continuous vegetable frying equipment with integral drum-type pots allows continuous frying and conveying of vegetables by rotating an internal stainless steel spiral (Adler-Nissen, 2007). With urbanization and the evolution of family structures, large group meals have placed new demands on industrially produced culinary egg products in terms of production capacity, efficiency, and product quality (Chen et al., 2020; Jia et al., 2024). However, when the above equipment is used for industrialized scrambled egg cooking, factors such as uncontrolled fire and uneven heat transfer often affect the final quality of the dishes (Fryer and Robbins, 2005; Li et al., 2023). During the scrambled egg process, the heat and mass transfer coefficients of the eggs change significantly as the temperature rises, which will result in the eggs at the bottom of the pan becoming cooked while the rest of the eggs remain liquid (Coimbra et al., 2006; Li et al., 2020). In addition, the

* Corresponding author. Institute of Food Science and Technology, Chinese Academy of Agricultural Sciences/Key Laboratory of Agricultural Product Processing, Ministry of Agriculture, Beijing, 100193, China.
** Corresponding author. Institute of Food Science and Technology, Chinese Academy of Agricultural Sciences/Key Laboratory of Agricultural Product Processing, Ministry of Agriculture, Beijing, 100193, China.
E-mail addresses: weiwensong8@163.com (W. Wei), 18910165989@163.com (C. Zhang).

https://doi.org/10.1016/j.crfs.2024.100948
Received 2 October 2024; Received in revised form 22 November 2024; Accepted 4 December 2024
Available online 7 December 2024

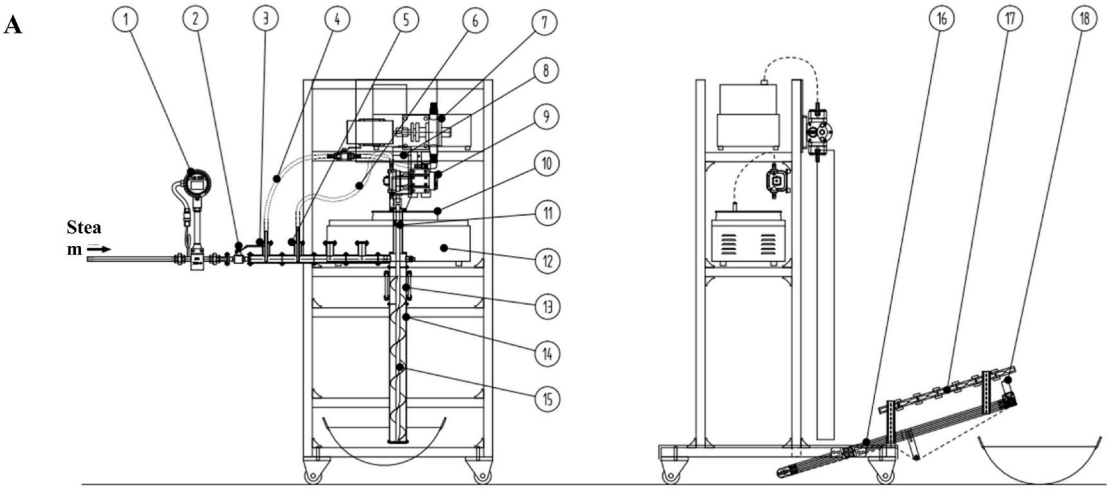

1. Steam flow metering unit 2. Steam control ball valve 3. Oil injection module 4. Oil Input tube 5. Egg injection module 6. Egg Input tube 7. Oil volume peristaltic pump 8. High temperature oil containers 9. Egg transfer pump 10. Egg wash container 11. Screw drive motor 12. Egg pre-heating box 13. High temperature resistant glass window 14. Egg block molding module 15. Spiral transmission module 16. Buffer conveyor belt 17. Heat dissipation module 18. Motors for driving belts

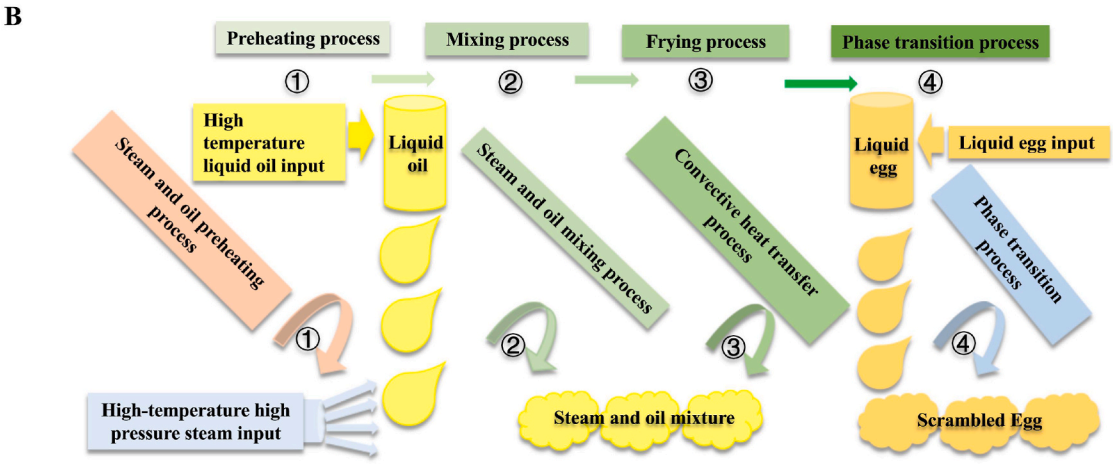

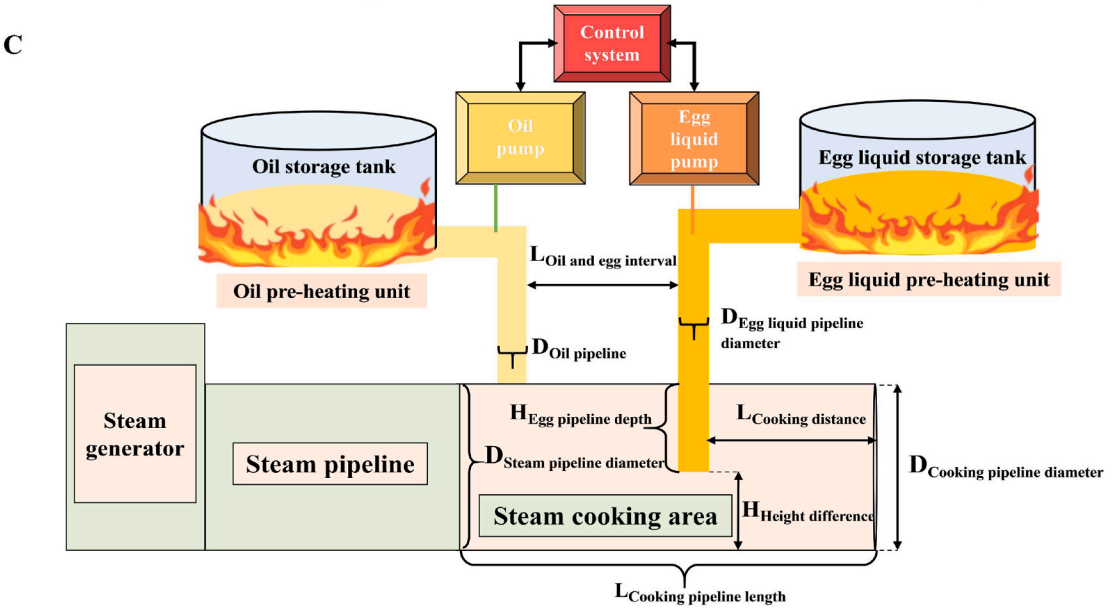

Fig. 1. Device structure and working principle. (A) Structure diagram of device for continuous scrambled eggs; (B) Operation principal diagram of steam scrambled egg device; (C) Structural diagram of continuous steam scrambled egg device.

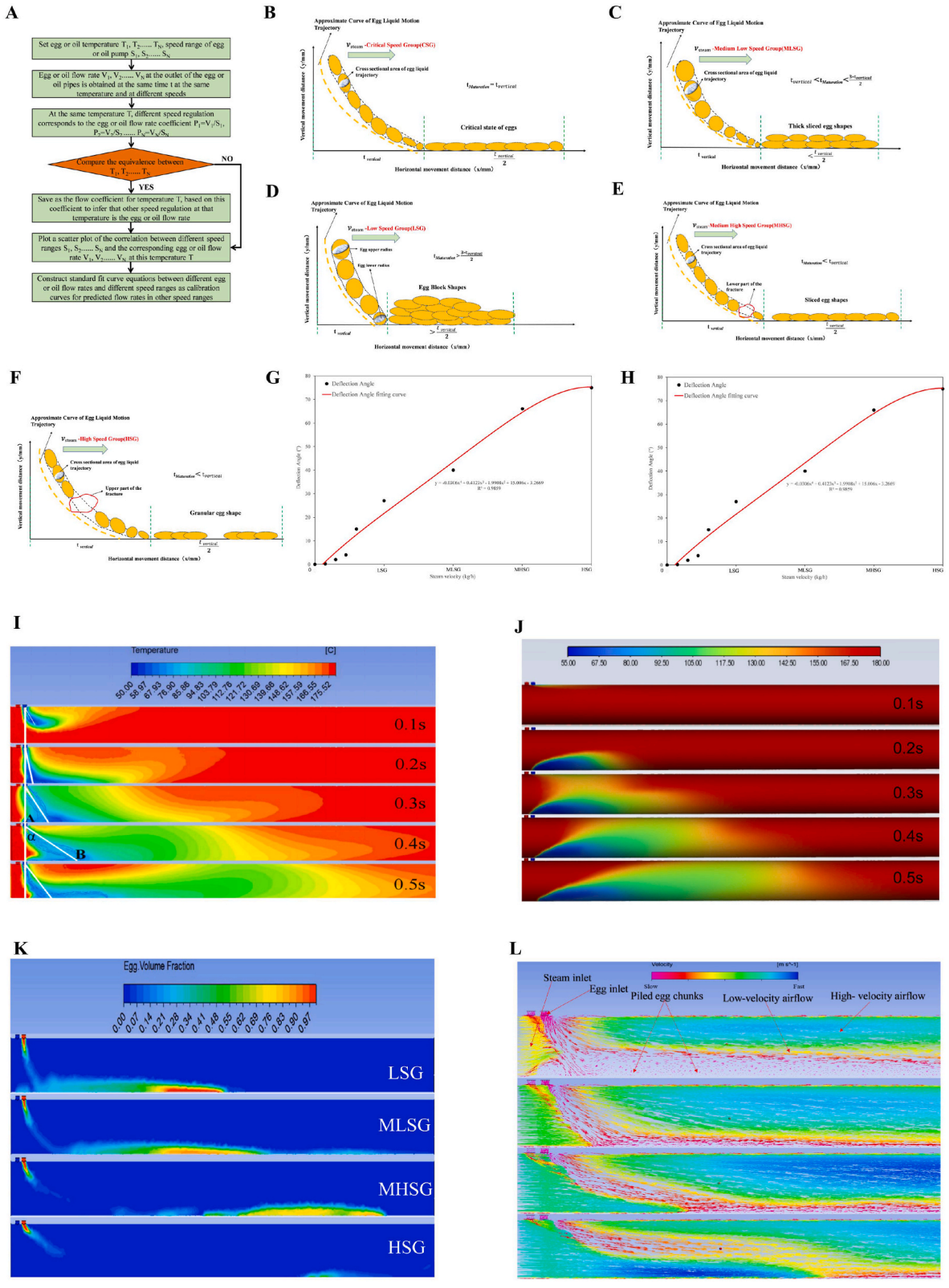

Fig. 2. (A) Flow chart of establishment of Calibration curve for Egg or Oil flow rate; Schematic diagrams of the trajectories of the egg in the horizontal and vertical directions at different steam velocities (B) CSG; (C) MLSG; (D) LSG; (E) MHSG; (F) HSG; Spatial Temperature Distribution (I) 1D and (J) 3D, and (G) Trajectory Changes in the Pipeline after Egg Liquid Lowering; (K) Horizontal trajectory distribution and (H) drop position distribution of egg at different steam velocities; and (L) Vector velocity distribution at various points inside the pipe after direct steam injection.

preparation of different dishes requires different shapes of scrambled eggs, e.g. scrambled rice requires broken eggs while scrambled eggs with tomatoes require block eggs. Therefore, the currently available equipment is unable to satisfy the diverse production needs of industrialized continuous scrambled eggs.

In the food industry, direct steam injection heating is attractive as a

direct heating technology that can greatly improve heat transfer efficiency (Sangsom and Inprasit, 2022). The steam is in direct contact with the product, condensing and releasing latent heat for rapid product processing, reducing product quality loss due to additional heat exposure (Wang and Zhao, 2023). In addition, direct steam injection heating prevents deterioration and clumping of raw material residues on the pipe walls, which can cause food safety hazards (Safavi Nic et al., 2020). In recent years, direct steam injection heating has been used in the dairy industry to minimize the denaturation of whey proteins and to extend product shelf life (Lee et al., 2017; Wang and Zhao, 2023). Currently, studies on direct steam injection during processing focus on the control of food quality, and few studies have been conducted on the transport trajectory and morphological changes of the materials after the steam has met them.

Therefore, in this paper, based on the direct steam injection principle, a continuous high-output scrambled egg device was developed to satisfy the demand for multi-form scrambled eggs needed for industrialized dishes. This device analyses the relationship between steam flow and velocity with the shape of scrambled eggs, determines the key parameters of the equipment, and validates the quality of scrambled eggs. In particular, the heat transfer process between steam and egg liquid was simulated by CFD to explore the effects of the pipeline flow trajectory of the egg liquid and the steam flow rate on the scrambled egg morphology. This device accurately regulates the flow of steam, egg, and oil to achieve multi-form scrambled egg production (block, thick slice, thin slice, and broken scrambled egg) and ensure uniformity of scrambled egg quality. Finally, compared with the traditional frying pan, the steam scrambled egg device was found to have high productivity, well-scrambled egg quality, and overall acceptability. This device provides technical and equipment support for industrialized continuous scrambled egg cooking and provides new insights for the development of other industrialized cooking equipment.

2. Materials and methods

2.1. Construction and operation of the device

The design of a continuous high throughput steam scrambled egg device is shown in Fig. 1A. The operating principle is as follows: When the high-temperature and high-pressure steam from the steam generator is released into the atmospheric air, a large amount of enthalpy will be released. Under the action of convective heat transfer, heat exchange occurs when high-temperature steam encounters the egg liquid, and the egg liquid changes from a liquid state to a solid egg mass after absorbing the enthalpy of steam and undergoing a phase change (Coimbra et al., 2006; Wang et al., 2024).

At the same time, the action of the hot oil at high temperatures encourages the migration of excess moisture. The moisture in the egg blocks is released into the air as steam to complete the scrambling process (Fig. 1B). This device can accurately adjust the key parameters of the four processes through the control system to complete the continuous production of steam scrambled eggs.

2.2. Establishment of calibration curves

The injection unit is the key to achieving continuous processing of steam scrambled eggs. In this device, the injection unit is divided into two parts: the egg liquid system and the oil system (Fig. 1C). Among them, the egg liquid storage tank is made of stainless steel (304). Circulating hot water (between 70 and 90 °C) is used to heat the egg liquid in the storage tank to ensure the temperature in 50–55 °C after preheating, preparing for the subsequent pump delivery.

This device uses the egg liquid pump model BT-600CA (Jieheng, China), the maximum flow rate of the pump is 1.68 L/m, and the maximum rotational speed is 600 r/min. In using a speed-regulated direct-current (DC) peristaltic pump to achieve egg liquid output, we established a speed-flow calibration curve for the egg injection system, providing a basis for precise control of the number of injections. At the pre-heating temperature of 55 °C, the flow rate of the tube outlet is measured at 20 different pump speeds, and the flow rate calibration curves are plotted at different speeds (Fig. 2A). Similarly, we establish the flow rate calibration curve of oil at 180 °C, with oil pump BY-353 (Jieheng, China), a maximum flow rate of 13 L/min and a maximum rotational speed of 600 r/min.

In this equipment, KRLUGB-DN15 vortex flowmeter combined with a graduated ball valve (0–90°) is used to achieve the adjustment of steam flow. By measuring the instantaneous steam flow rate at 8 different opening angles, the average flow rate at that opening angle is further calculated and a calibration curve of steam flow rate at different opening angles is established.

2.3. Size parameters for matured pipelines

This equipment adopts an electric heated steam generator (Norbes, China), with a capacity of 50 kg/h, a power of 36 KW, a rated working pressure of 1 Mpa, and a rated steam temperature of 184 °C.

$$q = h^{*}\left(T_{steam} - T_{Interface}\right) \tag{1}$$

In Newton's cooling law Eq (1), q is the heat throughput density (W/m^2). h is the convective heat transfer coefficient (W/(m^2*K)), satisfied by the Sieder Date formula (Eq (3)).(Subramanian, 2014) T_{steam} is the temperature (K) of steam, $T_{interface}$ is the surface temperature (K) of the medium in contact with saturated steam for heat exchange.

$$Nu = 0.027{*}R_e^{0.8}{*}P_r^{0.33}{*}\left(\frac{\mu}{\mu_W}\right)^{0.14} \tag{2}$$

$$h = \mathrm{Nu}{*}\frac{\lambda}{d} = 0.027{*}\frac{\lambda}{d}{*}\left(\frac{d{*}v_{steam}{*}\rho}{\mu}\right)^{0.8}{*}\left(\frac{C_p{*}\mu}{\lambda}\right)^{0.33}{*}\left(\frac{\mu}{\mu_W}\right)^{0.14} \tag{3}$$

Nu is the Nusselt number, R_e is the Reynolds number, P_r is the Prandtl number (Harding, 2018). Among them, λ is the thermal conductivity of the fluid (W m^{-1} K^{-1}), d is the diameter of the steam pipeline ($D_{steam\ pipeline}$, m), ρ is the fluid density (kg m^{-3}), μ is the viscosity of the steam fluid, μ_W is the viscosity of the steam fluid (m^2 s^{-1}) based on the temperature of the contact medium, Cp is the specific heat capacity of the fluid (J kg^{-1} K^{-1}), v_{steam} is the steam flow rate (m/s). The constants were determined by experiment.

The rated steam temperature T_{steam} and pressure P_{steam} (1 Mpa, 184 °C, 457.2K) of the steam generator are used in this equipment. Based on the steam frying of 1 kg liquid egg (whole egg from hen eggs), the pre-heating temperature of the egg liquid is set to 55 °C (328.1K). At this temperature, the specific heat capacity of the egg is about 3.2 kJ kg^{-1} °C^{-1}, and the target temperature is set to 100 °C. The $Q_{1kg\ egg\ liquid\ maturation}$ required for 1 kg of eggs to be heated from 55 °C (328.1K) to 100 °C (373.1K) satisfies Eq. (4), and $t_{maturation}$ required for 1 kg of liquid egg to mature satisfies Eq. (5).

$$Q_{1\ kg\ egg\ liquid\ maturation} = c{*}m{*}\Delta T = \frac{3.2\ kJ}{kg{*}^{\circ}C}{*}1\ kg{*}(100^{\circ}C - 55^{\circ}C) = 144\ kJ \tag{4}$$

$$t_{maturation} = \frac{Q_{1kg\ egg\ liquid\ maturation}}{Q_{heat\ flux}} = \frac{c{*}m{*}\Delta t}{h{*}(457.2K - 328.1K){*}S_{contact\ area}} \tag{5}$$

Where $Q_{heat\ flux}$ is the total heat exchange rate generated when steam encounters a certain mass of egg liquid, and $S_{contact\ area}$ is the surface area of convective heat transfer contact between a certain mass of egg and steam. The designed production capacity of this equipment is 1.5–2.5 t/d, and the $t_{liquid\ egg\ transfer}$ for transporting 1 kg eggs is 34 s (2.5 t) −72 s (1.5 t). $S_{contact\ area}$ should be maximized to meet 1 kg egg liquid filled with the maturation pipeline in 34 s. In actual operation, the steam flow

rate in contact with oil and eggs can cause energy loss resulting in a reduction in the steam flow rate.

To obtain a suitable maturation pipe diameter, the minimum maturation pipe diameter $D_{Steam\ pipe}$ should be selected. $L_{Maturation\ pipe}$ is 1800 mm in this study, and the density of the egg liquid ρ is 1.09 kg/m^3 at 55 °C. $D_{Steam\ pipe}$ is obtained according to Eq. (6).

$$D_{Steam\ pipe} = \sqrt{\frac{M}{\pi^* L_{Maturation\ pipe}{}^* \rho_{\ Egg\ liquid}}} = 26\ mm \tag{6}$$

In the actual scrambled eggs, the steam first contact with the oil, after the oil-egg distance transfer began to contact with the egg, due to the temperature of the hot oil is 180 °C and the temperature of the steam is close to the steam temperature, ignoring the effect of hot oil on the heat transfer of steam. (Fig. 1C) The D $_{egg\ liquid\ pipe}$ is 9.7 mm, currently, the egg liquid flow rate $v_{vertical\ egg}$ initial value to comply with Eq (7), for 0.39 m/s.

$$v_{vertical\ egg} = \frac{Q_{egg\ flow\ rate}}{\pi^* \left(\frac{D_{egg\ liquid\ pipe}}{2}\right)^2} \tag{7}$$

Similarly, in the actual process of scrambled egg and hot oil mass ratio of 5:1, the $D_{oil\ pipe}$ is 9.7 mm, the density of oil is about 0.92 g ml^{-1}, which can be derived that the $v_{vertical\ oil}$ is 0.085 m/s, the flow rate of the oil is 6.3 mL/s. Fig. 1C in the $L_{oil\ egg\ distance}$, $H_{egg\ pipe\ depth}$ can be adjusted according to the actual situation, to reduce the influence of the oil on the steam, which can maximize the direct contact between the steam and the egg, $H_{height\ difference\ 2}$ can be approximated as equal to the $D_{steam\ pipe}$.

2.4. Determination of steam flow rates for different egg masses

2.4.1. Establishment of the correspondence between steam flow and egg mass

Under the condition of releasing the same steam pressure and temperature, different steam speeds of the steam generator will produce different impacts on the egg liquid (Hoznedl and Gregor, 2020), dividing the egg liquid into droplets of different shapes, which form different shapes of egg blocks after maturation. The gas flow rate on the liquid impact and the resulting acceleration are accorded with Eq. (8).

$$\left.\begin{aligned} F_{impact\ force} &= \rho_{steam}{}^* S_{contact\ area}{}^* v_{steam}{}^2 \\ \boldsymbol{a} &= \frac{F_{impact\ force}}{\rho_{egg\ liquid}{}^* Q_{egg\ liquid\ flow\ rate}{}^* t_{\ egg\ liquid\ transfer\ 1}} \end{aligned}\right\} \tag{8}$$

$F_{impact\ force}$ is the impact force on the egg liquid, ρ_{steam} is the density of steam at a certain temperature, V_{steam} is the flow rate of the steam, and $\boldsymbol{a}$ is the acceleration generated. In the actual frying process, the egg liquid is transmitted in the vertical direction and horizontally under the steam blowing. Assuming that the change of the impact force of the steam on the egg liquid in the horizontal direction is negligible, i.e., the $F_{impact\ force}$ is constant, then the trajectory of the egg in the vertical and horizontal directions given moment satisfies Eq (9).

$$\left.\begin{aligned} Y_{transfer} &= H_{height\ difference\ 2} - v_{vertical\ egg\ speed}{}^* t + \frac{1}{2}\boldsymbol{g}^* t^2 \\ X_{transfer} &= v_{horizontal\ egg\ speed\ 0}{}^* t + \frac{1}{2}\boldsymbol{a}^* t^2 \end{aligned}\right\} \tag{9}$$

Where $Y_{transfer}$ and $X_{transfer}$ represent the trajectory of the egg liquid in the vertical and horizontal directions during the falling time, and $v_{horizontal\ egg\ speed\ 0}$ is zero. The relationship between $Y_{transfer}$ and $X_{transfer}$ is obtained to satisfy Eq. (10).

$$Y_{transfer} = H_{height\ difference\ 2} - v_{vertical\ egg\ speed\ 0}{}^* \sqrt{\frac{2^* X_{transfer}}{\boldsymbol{a}}} - \frac{\boldsymbol{g}^* X_{transfer}}{\boldsymbol{a}} \tag{10}$$

Under the effect of vapor flow rate, the egg liquid will show a curved surface distribution inside the pipe, coupled with the Rayleigh-Plateau instability of the liquid (Mead-Hunter et al., 2012), leading to the formation of a continuous ellipsoid-like shape under the effect of gravity (Fig. 2B–E). The area of this surface in space approximately satisfies Eq. (11).

$$\left.\begin{aligned} S &= S_0 + \int_0^X \pi^* (R_{up} + R_{low})^* \sqrt{1 + \left(\frac{v_{vertical\ egg\ speed}}{\sqrt{2^* X_{transfer}{}^* \boldsymbol{a}}} + \frac{\boldsymbol{g}}{\boldsymbol{a}}\right)^2}\, dX \\ S_0 &= \pi^* \left(R_{upper}{}^2 + R_{lower}{}^2\right) \end{aligned}\right\} \tag{11}$$

In the actual transfer process, the overall effective time of $X_{transfer}$ is a fixed value, and the final curved surface S of the egg liquid satisfies Eq. (11).

$$S = S_0 + \pi^* (R_{upper} + R_{lower})^* \left(\frac{1}{2}\boldsymbol{a}^* t^2 + \frac{v^2_{Vertical\ Egg\ Speed\ 0}}{2^* \boldsymbol{a}} + \frac{v_{Vertical\ Egg\ Speed\ 0}{}^* \boldsymbol{g}}{\boldsymbol{a}^* t} + \frac{t^* \boldsymbol{g}^2}{2^* \boldsymbol{a}}\right. \tag{12}$$

t is equal to the time for the egg to fall vertically in the vertical direction during the actual ripening process. Combined with Eq. (8), it can be concluded that the magnitude of the steam impact causes the same egg volume to exhibit different contact areas. Assuming that the target egg block volume is $V_{target\ egg\ block}$, when the egg liquid in the $t_{egg\ liquid\ transfer\ (1)}$ in the vertical direction out of the egg liquid flow rate is constant, the steam flow rate impact force and the target egg block can be derived from the relationship between Eq. (13).

$$F_{impact\ force} = \frac{D_{Maturation\ Pipeline}}{\sqrt[3]{\frac{3^* V_{target\ egg\ block}}{4^* \pi}}}{}^* \left(\frac{2^* X_{\ transfer}}{t_{egg\ liquid\ transfer\ (1)}{}^2} + 2^* \int_0^{2^* \sqrt[3]{\frac{3^* V_{target\ egg\ block}}{4^* \pi}}} \sigma^* L dL\right) \tag{13}$$

σ is the surface tension coefficient of the egg liquid (N/cm), and L represents the length of the spherical cross-section of the target egg mass moving in the horizontal direction(Bohr and Scheichl, 2021). Combined with Eqs. (8)–(10), the steam flow rate was adjusted to control different target egg block sizes at a fixed egg flow rate and oil flow rate.

At different steam flow rates, the variation of the egg contact area S affects the egg ripening time $t_{Maturation}$. Under gravity, the egg drop time $t_{vertical}$ is a fixed value that can be divided into the following cases under different steam flow conditions.

(1) When the steam velocity is the Critical Speed Group (CSG), $t_{Maturation} = t_{vertical}$ (Fig. 2B). In the time of $t_{vertical}$, the steam will be cooked egg liquid completed, cooked egg liquid at the bottom of the pipe in the same acceleration a, and after $t_{vertical}/2$ to complete the transmission of cooked egg liquid. At this point, a total of $3 * t_{vertical}/2$ is required from the start of egg transfer to the bottom, which is defined as the critical maturation time without stacking. The cooked egg spreads out flat at the bottom of the pipe and continues to be transported forward by the steam flow rate.

(2) When the steam velocity is Medium Low Speed Group (MLSG), i.e., $t_{vertical} < t_{Maturation} < 3^* t_{vertical}/2$ (Fig. 2C). The $t_{Maturation}$ prolonged, the egg fell to the bottom of the steam pipe is not yet completely cooked, and less than $t_{vertical}/2$ to complete the cooking. The subsequent egg and the unsolidified egg at the bottom of the pipeline show the flat stack. Finally, the egg under the action of steam heat denaturation solidified into a thick slice.

(3) When the steam velocity is Low Speed Group (LSG), the $t_{Maturation} > 3^* t_{vertical}/2$ (Fig. 2D). Currently, the $t_{Maturation}$ is longer, the egg has fallen to the bottom of the steam pipe is not yet completely cooked. After $> t_{vertical}/2$ of the time the egg to complete

maturation, the subsequent egg and previous unsolidified egg at the bottom of the pipeline show many stacked cases, and finally in the steam heat transfer effect of denaturation and solidification into a stacked block.

(4) When the steam velocity is Medium High Speed Group (MHSG), $t_{Maturation} < t_{vertical}$ (Fig. 2E). The $t_{Maturation}$ is shorter than the critical flow rate, the egg has completed cooking before falling to the bottom of the steam pipe. And the egg has finished solidifying without stacking within $t_{vertical}/2$. When the flow rate exceeds the critical flow rate causing the egg to break from the bottom, both the broken portion of the egg and the unbroken portion have completed cooking, and finally continue to be transported under the action of the steam flow rate, at which time the overall shape of the egg is flaky after cooking.

(5) When the steam velocity is High Speed Group (HSG), $t_{Maturation} < t_{vertical}$ (Fig. 2F). The $t_{Maturation}$ is shorter than the critical flow rate, the egg still does not completely fall to the bottom of the steam pipeline and has been completed all cooked. From the egg liquid pipeline just after the flow out of the steam at high speed under the action of the fracture, cooked after the formation of granular morphology, in the steam flow rate under the action of rapid transmission and then stacked, the overall shape of the egg after cooking presents a fine crumbly granular shape.

Based on the above relationship between egg shape and steam flow rate, it can be deduced that the steam frying of block, thick slice, thin slice, and broken egg can be achieved when the steam flow rate is 1.85 kg/h (LSG), 2.82 kg/h (MLSG), 3.93 kg/h (MHSG), and 4.85 kg/h (HSG), which can satisfy the requirements of egg dishes processing.

2.4.2. CFD simulation of different steam flow rates and egg morphology

This paper used numerical simulation combined with the Computational Fluid Dynamics (CFD) method to carry out the analysis of steam/egg liquid two-phase flow. After calculating the *Re*, we know that the fluid state in the pipeline is turbulent, and the steam pipeline is a regular model, so k-ε standard turbulence model is chosen. Space Claim was used to establish the simulation model of the egg steam pipeline to study the trajectory of egg liquid entering the pipeline under different steam velocities.

· Initial conditions

The pipe length was shortened without affecting the simulation, and the steam pipe length was 1000 mm with tetrafluoroethylene sprayed on the inner wall and a friction factor of 0.05. In addition, the density of egg liquid was 1.09 g/cm^3, surface tension 0.05 N/m, viscosity 0.15 kg/(m·s), thermal conductivity 2 W/(m·K), specific heat capacity 4000 J/(kg·K), initial temperature 55 °C, and flow rate 0.39 m/s. The density of edible oil was 0.92 g/cm^3, surface tension 0.07266 N/m, viscosity 0.025 kg/(m·s); thermal conductivity 0.2, specific heat capacity 2300 J/(kg·K), initial temperature 180 °C, flow rate 0.085 m/s. Steam pressure 1 MPa, 184 °C, at steam flow rates of 1.85, 2.82, 3.93, 4.86 kg/h respectively CFD simulations were performed.

· Boundary conditions and mesh

Time-dependent entrance velocity boundary conditions are defined to simulate sudden increases in entrance velocity at specific points in time. The inlet velocity is 100.0 m/s for simulation times between 2.0 and 2.1 s, between 3.0 and 3.1 s, or between 4.0 and 4.1 s. For other times, the inlet velocity is 4.0 m/s. Using this dynamically adjusted inlet velocity setting, the unsteady state conditions of real-world operation can be simulated more realistically, resulting in more accurate simulation results. No-slip boundary conditions are applied to this CFD model. The 3D modeling graphs, mesh graphs, and build sections are shown in Supplementary Fig. S1.

Table 1
Two different mesh elements (5 mm or 4 mm) and results.

Meshes	Monitoring point temperature (°C)	Average outlet temperature (°C)	Surface average temperature (°C)
197889	129.57230	129.21749	126.10120
312819	138.04141	136.68389	130.88985

According to the meshing standard, to ensure the simulation effect, the bending place, groove, and other positions are densely meshed with a grid size scale of 1 mm, and to reduce the calculation volume, the rest of the parts are sparsely meshed with a grid size scale of 5 mm, and the total number of meshes is 197889.

Next, mesh independence was verified. The dense mesh size of 1 mm was kept constant, and the sparse mesh size was scaled to 4 mm for a total of 312819 mesh elements. The average temperature values at the monitoring point, outlet, and all surfaces were recorded for two different mesh elements and the results are shown in Table 1.

The error in the values of the two meshes is between 3% and 7%, the temperature fluctuations are relatively close and the influence of the mesh on the results is within acceptable limits. Although finer meshes (e.g., 4 mm) may provide higher computational accuracy, this increase in accuracy was not significant in our validation. To save computational resources, the 5 mm mesh was chosen for subsequent calculations.

· Governing equations

In the CFD simulation of this model, the governing equations involve the following formulations to describe the fluid flow, heat transfer, and phase change processes.

- The mass conservation equation:

$$\frac{\partial \rho}{\partial t} + \nabla(\rho \boldsymbol{u}) = 0 \tag{14}$$

- The momentum conservation equation:

$$\frac{\partial(\rho u)}{\partial t} + \nabla(\rho \boldsymbol{u}\boldsymbol{u}) = -\nabla p + \nabla(\mu \nabla \boldsymbol{u}) + \rho \boldsymbol{g} \tag{15}$$

- The phase transition model:

$$\left.\begin{aligned} \frac{\partial f}{\partial t} + \boldsymbol{u}\nabla f = S_f \\ S_f = \frac{f(t)}{\tau} \end{aligned}\right\} \tag{16}$$

- The energy conservation equation:

$$\rho c_p \left(\frac{\partial T}{\partial t} + \boldsymbol{u}\nabla T\right) = \nabla(k \nabla T) + L\frac{\partial f}{\partial t} \tag{17}$$

- Volume of fluid method:

$$\frac{\partial a_i}{\partial t} + \nabla(a_i \boldsymbol{u}) = 0 \tag{18}$$

Where ρ is the fluid density, u is the velocity vector, $\rho \boldsymbol{u}$ is the momentum density, $-\nabla p$ is the pressure gradient force, $\nabla(\mu \nabla u)$ is the viscous force, $\rho \boldsymbol{g}$ is the gravity term, f is the phase variable (0 for liquid, 1 for solid), S_f is the phase transition source term and is usually temperature and latent heat dependent. $f(T)$ is a function of temperature. τ is the characteristic time scale to describe the time scale of the phase transition process. ρc_p is the heat capacity, T is the temperature, k is the thermal conductivity, L is the latent heat, $\frac{\partial f}{\partial t}$ is the rate of change of the

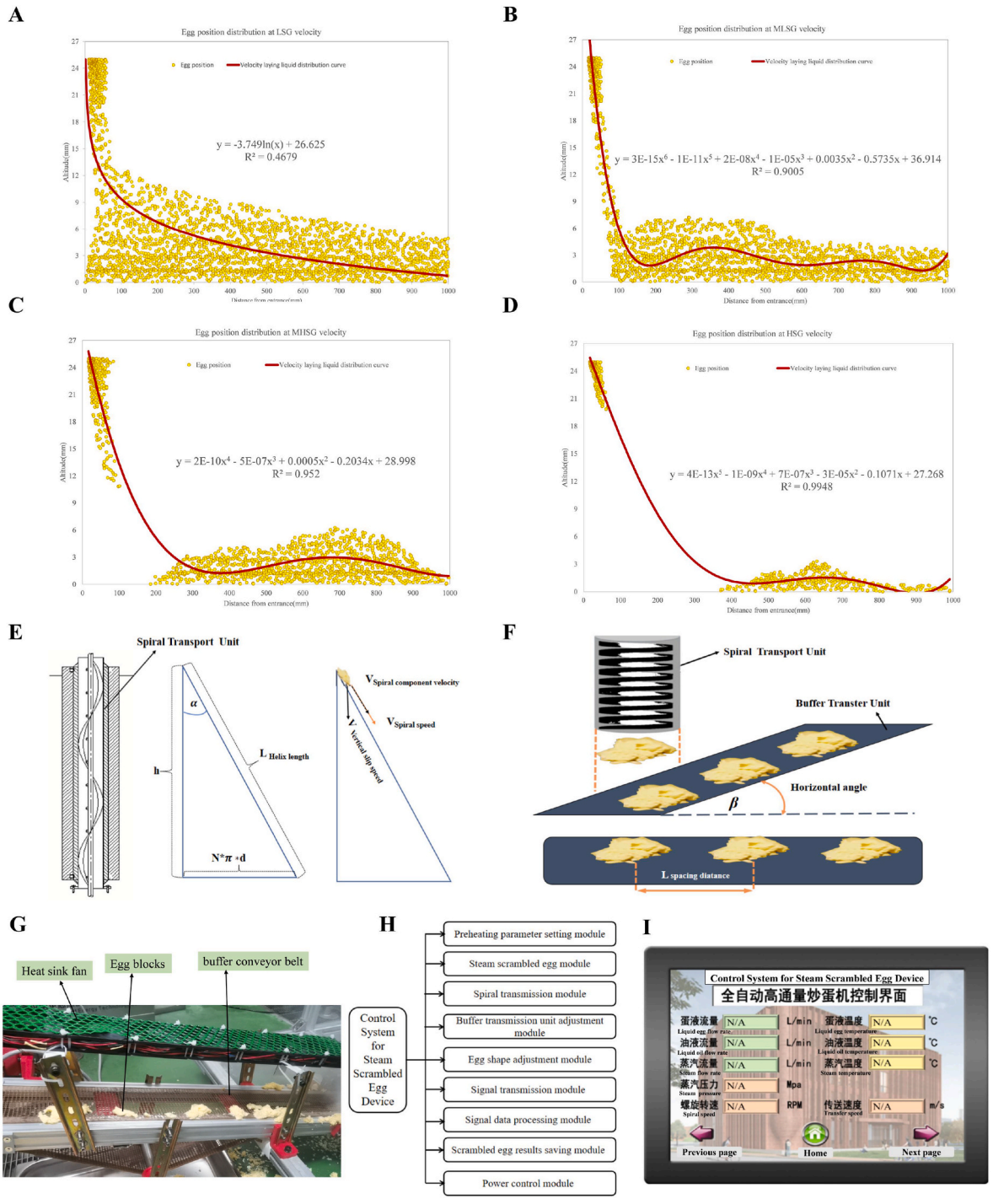

Fig. 3. Egg distribution profiles at different direct steam injection speeds (A) LSG; (B) MLSG; (C) MHSG; (D) HSG; (E) Motion Analysis of eggs on Spiral transmission Unit; (F) Physical diagram of egg buffer transmission unit; (G) Egg block transfer physical diagram; (H) The main module composition of the system; (I) The software interface of the control system.

phase variable with time and denotes the internal heat source of the fluid. a_i is the volume fraction of phase *i*.

As shown in Fig. 2I and J, the temperature of the egg liquid changes slowly during the initial falling stage (0–0.2 s). However, after 0.2 s, the temperature at the outlet of the egg liquid rises to the denaturation temperature (≥76 °C) and then remains stable. Under the influence of direct steam injection, the egg blocks pile up on the right side of the descending point and move toward the outlet of the pipeline. The line connecting the center point B at the top of the falling egg column with the center point A at the egg outlet (white solid line in Fig. 2I), and the angle α with the vertical direction is taken as the deflection angle of the egg. During the process from low to high speed, the deflection angle α increases with the increase of the steam flow rate (Fig. 2G).

During the initial falling stage, the column of egg liquid was pushed by the steam and swayed greatly until reaching the maximum deflection angle. After it completely falls, the falling trajectory tends to be stable. Based on the deflection angle, it is assumed that at increasing steam flow rates, the egg will be blown into particles until eventually full of the entire pipe (Fig. 2H–K).

From the simulation results (Fig. 2K), the location of the main region

of the Egg Volume Fraction (EVF) drop point (red and yellow regions in Fig. 2K), in the pipeline shifts backward as the steam flow rate increases from low to high speeds. As the flow rate increases, the accumulation point of egg liquid inside the pipe is closer to the outlet. As the steam flow rate increases from LSG to HSG, the egg liquid is blown apart inside the pipe and becomes a smaller percentage of volume in space, and the accumulation point is closer to the outlet.

As the steam flow rate increases, the interceptions in the piping decrease significantly at the same moment (Fig. 2H). When the flow rate is slow, the egg drop point is away from the outlet, and the pile adheres to the inner wall, gradually forming egg blocks and pieces; When the flow rate is faster, the drop point is closer to the outlet with egg being blown apart into small particles that move quickly toward the outlet (Figs. 2L and 3A–D).

As shown in Figs. 2L and 3A–D, eggs in the LSG and MLSG were only slightly deflected during their descent and the egg column remained continuous. And the eggs completely fell to the bottom of the pipe and appeared to pile up, and the block and flake eggs slid out along the pipe under the steam thrust. At MHSG and HSG velocities, eggs were blown right side up and egg columns broke immediately after descending. At MHSG, the egg column partially broke at the top, and as the flow rate increased the egg column broke at the bottom. At HSG, the egg completes its maturation in the steam and falls to the bottom of the pipe in the form of thin slices. However, the egg changes to a granular solid, moves to the right, and slides quickly out of the pipe during MHSG.

2.5. Unit and control system design

2.5.1. Egg block forming and spiral transfer unit

To convert egg masses from horizontal to vertical conveying, we designed an egg mass forming and screw conveying device. In this experiment, the spiral transfer unit consists of the spiral drive motor, coupling, spiral conveying blade, and vertical conveying cylinder, and the inner walls of all pipes are sprayed with tetrafluoroethylene (PTFE, Fig. 3E). In this experiment, the spiral transfer height is 1 m, the diameter of the vertical conveying cylinder is 46 mm, the spiral turns are 2, and the spiral rise angle is 30°. The transfer velocity of the egg blocks ($v_{vertical\ slide\ speed}$, Initial value is 0) consists of the combined velocity of the component v_1 on the spiral incline and the self-carried velocity v_2 of the spiral blades (Eq. (19)).

$$\left.\begin{aligned} v_2 &= \frac{R_{rpm}*\pi*h}{60} \\ v_1 &= v_{vertical\ slide\ speed\ (0)} + (g*\cos(\alpha) - \mu*g*\sin(\alpha))*t \end{aligned}\right\} \tag{19}$$

To transfer the egg mass to the bottom quickly, the minimum speed of the screw conveyor blades, R, needs to satisfy Eq. (20).

$$\left.\begin{aligned} v_2*t + \frac{1}{2}*v_1*t &= \frac{h}{\cos(\alpha)} \\ \tan(\alpha) &= \frac{2*\pi*d}{h} \end{aligned}\right\} \tag{20}$$

In Eq. (15), the maximum time t used in the spiral transfer is set to be about 200 ms to satisfy the capacity of steam scrambled eggs. μ is the friction coefficient of the spiral blade (PTFE) about 0.05. Therefore, the minimum speed of the screw drive motor is 99 rpm/min.

2.5.2. Buffer transfer unit design

The buffer transfer unit spreads the output egg blocks uniformly and rapidly cools down the scrambled egg blocks with the heat dissipation module to avoid localized overheating that produces ferrous sulfide leading to blackened and green eggs(Shahbaz et al., 2018). The buffer transfer unit is a gap transfer belt in the horizontal direction at an angle β, the heat dissipation module is set at the top of the parallel direction of the transfer belt, and the overall power relies on the belt drive motor (Fig. 3F and G). To prevent stacking egg blocks, the minimum belt transfer speed $v_{conveyor\ belt}$ needs to satisfy Eq. (16).

$$v_{conveyor\ belt} \geq \frac{l_{transmission\ distance}}{t} = \frac{d}{\cos(\beta)*t} \tag{21}$$

In Eq. (21), the $l_{transmission\ distance}$ is the shortest spacing of egg blocks in the direction of belt rise, t is egg block transfer time, which is 200 ms, d is the spiral transfer cylinder diameter, which is 46 mm, and β is 15°. Therefore, the minimum speed is calculated to be 30.2 cm/s, and this experiment takes 31 cm/s.

2.5.3. Overall control system design

The device is based on Raspberry Pi module, Linux system, QT Meta Language design software structure. The software structure design is shown in Fig. 3H. The control interface of the software is shown in Fig. 3I which is divided into four main parts. The control software enables the setting of key parameters at different capacities; real-time monitoring and alerting of steam pressure and temperature; and recording and information storage of production parameters.

2.6. Performance Verification

To verify the performance of the continuous high-throughput steam device, eggs scrambled in an automatic frying pan were used as the Control Group (CG). The steam flow rate was divided into four experimental groups: LSG (1.85 kg/h), MLSG (2.82 kg/h), MHSG (3.93 kg/h), and HSG (4.86 kg/h). In this case, the egg flow rate in the device was set to 29 ml/s and the oil flow rate was 6.30 ml/s. The oil used to scramble the eggs is homogenized peanut oil (Jinlongyu, Yihai Kerry Group, China). Eggs used were from local markets (Beijing, China), and whole eggs were used for the scrambled validation experiment. The egg-to-oil mass ratio was 5:1 in all groups, and the pre-heating temperatures of the egg and oil before cooking were set at 55 °C and 180 °C, respectively.

In addition, the fully automatic frying pan was selected with a rated power of 0.75 KW, stirring frequency of 30 times/min, and effective space for frying was 1/5 of the whole. The time was recorded throughout, and at the end of the experiment, the eggs were allowed to stand for 1 h. After the eggs were returned to room temperature (25 °C), 30 g of each group was taken and stored in a sealed bag to complete the subsequent determinations.

2.6.1. Scrambled egg size and volume

Since the scrambled egg blocks are irregular in shape, to simplify the calculation process, the egg shape is approximated as an ellipsoid. Vernier calipers were used to measure the length, width, and thickness of the egg block and half of each dimension was taken to represent the long half-axis a, middle half-axis b, and short half-axis c, respectively, and the specific calculation formula was as in Eq. (22).

$$\left.\begin{aligned} F &= \frac{a-c}{a} \\ P &= \frac{\sqrt{a^2-c^2}}{a} \\ P' &= \frac{\sqrt{a^2-c^2}}{c} \\ V &= \frac{4*\pi*a*b*c}{3} \end{aligned}\right\} \tag{22}$$

F is used to evaluate the degree of flattening of the ellipsoid. P and P' are the ratio of the focal point of the ellipsoid from the center to the ellipsoid radius.

2.6.2. Color measurement

Referring to the Shahbaz method, L^*, a^* and b^* were measured

Table 2
The criteria for judging the overall color difference.

ΔE	Results
0–0.25	Perfect match
0.25–0.5	Acceptable match
0.5–1.0	Minor to moderate variance
1.0–2.0	Moderate variance
2.0–4.0	Wide variation
Above 4.0	Huge variation

directly for each group of samples to calculate ΔE with the formula shown in Eq. (23) (Shahbaz et al., 2018).

$$\Delta E = \sqrt{\Delta L^{*2} + \Delta a^{*2} + \Delta b^{*2}} \quad (23)$$

The criteria for judging the overall color difference are shown in Table 2.

2.6.3. Texture profile analysis

The textural properties of the samples were determined using texture profile analysis (TPA) and the results were expressed as a parallel average of three measurements. Measurement conditions: Probe type P/36R, pre-test speed 2 mm/s, test speed 1 mm/s, post-test speed 2 mm/s, trigger force 10 g, deformation 70%.

2.6.4. Quality sensory evaluation

Referring to the method of Shahbaz (Shahbaz et al., 2018), 12 experienced sensory evaluators were selected to evaluate and score the

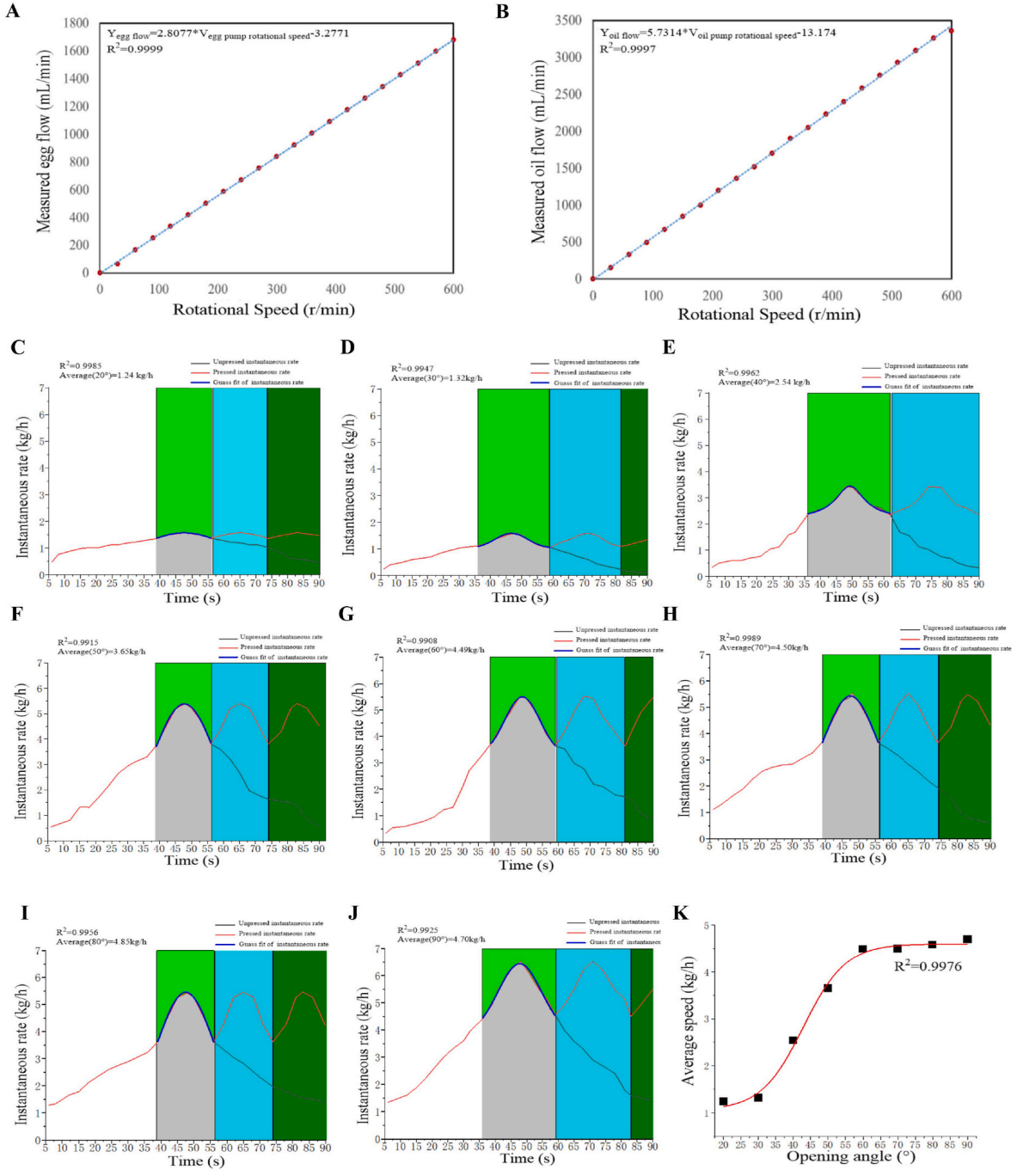

Fig. 4. Calibration curve of (A) egg flow rate and (B) oil flow rate at different rotating speeds; Rate dynamics change curve of steam ball control valve at different opening angle: (C) Opening angle at 20°, (D) 30°, (E) 40°, (F) 50°, (G) 60°, (H) 70°, (I) 80°, (J) 90°; and (K) steam rate calibration curves with different openings.

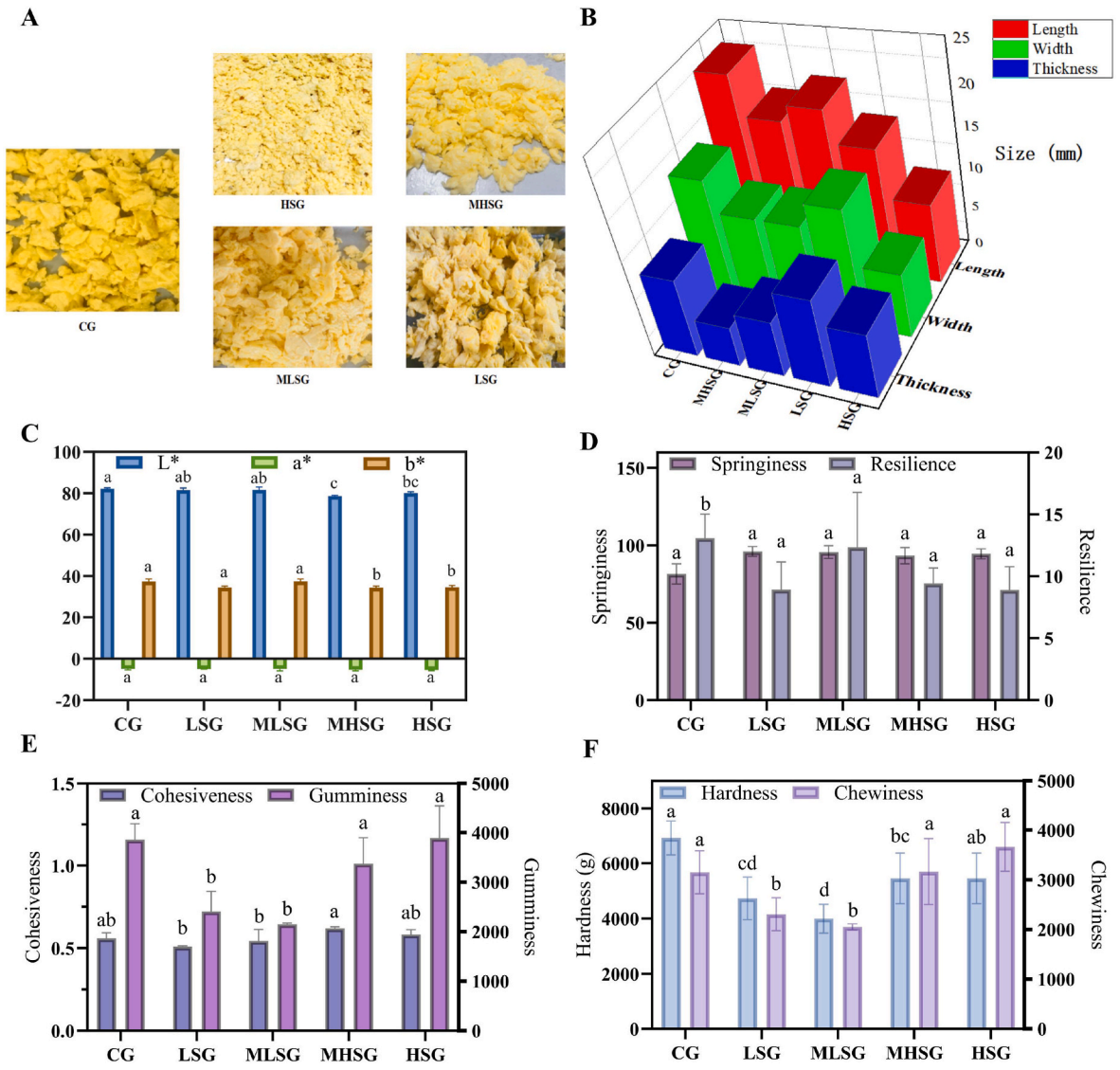

Fig. 5. (A) Physical images and (B) Average size of scrambled eggs between control group and experiment group; Comparison of (C) egg color and egg (D) Springiness, Resilience, (E) Cohesiveness, Gumminess, (F) Hardness and Chewiness between the reference group and the experiment groups. Different low-case letter indicates that mean values are significantly different ($p < 0.05$).

samples. Before changing samples, the evaluator rinses his/her mouth to remove the sample from the mouth.

2.7. Data analysis

Mean values and standard deviations were calculated from the three replicates for each treatment. Differences were estimated by IBM SPSS Statistics 26 analysis of variance (ANOVA) followed by Duncan's test, with $p < 0.05$ considered significant.

3. Results and discussion

3.1. Establishment of calibration curves

As shown in Fig. 4A and B, at the same temperature, different rotational speeds corresponding to the flow coefficient $P_{egg\ liquid}$ is about 2.81, corresponding to the flow coefficient P_{oil} is about 5.73. The calibration curves are all consistent with the linear law of change, and the fitting equations satisfy Eqs. (24) and (25), respectively.

$$Y_{egg\ liquid(i)} = P_{egg\ liquid} * V_{egg\ pump\ (i)} + Y_1 = 2.8077 * V_{egg\ pump\ (i)} - 3.2771 \quad (24)$$

$$Y_{oil(j)} = P_{oil} * V_{oil\ pump\ (j)} + Y_2 = 5.7314 * V_{oil\ pump\ (j)} - 13.174 \quad (25)$$

$Y_{egg\ liquid\ (i)}$ and $Y_{oil\ (j)}$ are the real-time egg and oil flow rates, $V_{egg\ pump\ (i)}$ and $V_{oil\ pump\ (j)}$ are the real-time egg and oil pump speeds, the Y_1 and Y_2 are corrections for the negative pressure overcome by the egg and oil pumps initially, and the calibrated curves can be used for subsequent prediction of egg liquid and oil flow at any speed.

The instantaneous rate of steam due to different ball valve openings shows a first increase and then a decrease, and the instantaneous rate reaches the peak at 50 s and then decreases to the initial level, and the rate trend is accorded with the Gaussian function distribution. Steam generators with varying degrees of pressure drop can cause a drop-in instantaneous rate. To ensure a constant steam flow rate, the steam generator needs to be pressurized in real time to ensure that the steam rate error does not exceed 1%. The red line reflects the change in the instantaneous value of the steam rate after repressurization, and the instantaneous rate after a fixed period of repressurization shows a periodic state of change (Fig. 4C–J).

Table 3
Comparison results of scrambled egg size between control group and experiment groups.

Groups	Volume (mm^3)	Length (mm)	Width (mm)	Thickness	Flat rate	First eccentricity	Second eccentricity
					F	*P*	*P'*
Control	1976.82	23.20	16.05	10.14	0.56	0.90	2.06
LSG	573.43	18.12	12.07	5.01	0.72	0.96	3.48
MLSG	883.11	20.02	11.99	7.03	0.65	0.94	2.67
MLHG	1405.47	16.11	15.10	11.04	0.32	0.73	1.06
HSG	356.30	10.20	8.15	8.19	0.20	0.60	0.74

The mean value of the rate at a given opening is obtained by fitting the kinetic curve (solid blue line) for instantaneous rates over 70% of the peak, and the average rate calibration curve is plotted for different openings. The average rate change at 20° and 30° is small, and the average rate from 60° to 90° shows a steady state, and the calibration curve satisfies Eq. (26).

$$y_{steam\ speed} = A_2 + \frac{(A_1 - A_2)}{1 + e^{\left(\frac{x_{opening\ \ degree} - x_0}{dx}\right)}} = 4.60 + \frac{1.05 - 4.60}{e^{\left(\frac{x_{opening\ \ degree} - 42.92}{6.07}\right)}} \quad (26)$$

The steam rate averages for openings 30°–60° are approximately linear which can be used as an effective range for steam flow control. In addition, the mean values at 60°–90° remained stable and unchanged may be since when the high temperature and high-pressure steam is released to atmospheric pressure, the fluid inside the pipe is subjected to resistance and friction, resulting in a restricted increase in flow rate (Zhao et al., 2023). In addition, the fluid flow in the pipeline is also affected by factors such as Reynolds number and flow pattern. The flow rate will not increase linearly after increasing the flow rate in the same pipeline.

3.2. Comparison of production capacity

In this experiment, the total cooking time of 20 L eggs in the CG was about 30 min, and the equipment utilization rate was 60%, then the production capacity of the automatic frying pan was about 24 kg/h. The capacity of the continuous high-throughput steam device is about 104.4 kg/h (2.5 t/day, 24 h), which is 4.35 times the capacity of the automatic scrambler. Therefore, the use of high-throughput steam devices can significantly improve the production efficiency and capacity of egg products.

3.3. Analysis of volume discrepancies in scrambled eggs

The egg blocks cooked in the HSG were the smallest in size and granular, the MHSG showed egg masses like the GC results, whereas the samples from both the MLSG and LSG were in the form of flakes (Fig. 5A). CG has the largest egg mass volume, MLHG has the second largest volume and HSG has the smallest egg mass volume. In addition, the flatness and *P* of the egg blocks for LSG and MLSG were higher than those of the other groups (Table 3). These parameters determine the overall flat flake shape of the scrambled egg size (Fig. 5B) (Lian et al., 2024)

The results agree with the previously derived relationship between egg mass shape and steam flow velocity and the CFD simulations. When the egg and oil flow rate is constant, the greater the steam flow rate, the greater the force released to the egg-liquid interface, and the smaller volume of the egg liquid is swept, under the steam heat flow, it will be condensed and solidified into particles. Instead, part of the egg will be set into blocks and the others will be set into slices. When the steam flow rate is reduced to insufficient to blow away the interface completely, the egg will solidify into flakes.

Table 4
Comparison results of Color between control group and experiment groups.

Groups	ΔL	Δa	Δb	ΔE
LSG	−0.6133	−0.0767	−0.0307	0.6188
MLSG	−0.5133	−0.0033	0.0433	0.5152
MHSG	−3.5333	−0.5067	−2.9667	4.6414
HSG	−2.0767	−0.6100	−2.7133	3.4709

3.4. Analysis of color in scrambled eggs

Color is one of the key organoleptic indicators that affect scrambled eggs. In terms of the L^*, MHSG and HSG showed a significant difference from the other groups ($p < 0.05$). The results showed that higher steam flow rates increased the degree of mixing of the oil and the eggs, leading to differences in water evaporation rates from the egg blocks, and thus affecting the L^* (Fig. 5C).

Prolonged heating of eggs leads to protein structural changes, where disulfide bonds break and react with vitellogenin to produce hydrogen sulfide which combines with ferrous ions in the yolk to produce green ferrous sulfide, leading to the formation of localized green patches internally(Shahbaz et al., 2018). On the a^*, the difference between the groups was not significant, indicating that there was no significant overheating in either group.

b^* represents the yellowness of scrambled eggs, which is mainly determined by the amount of lutein, zeaxanthin, and carotenoids in the egg mixture (Dansou et al., 2023). The yellowness values of MHSG and HSG were significantly lower than other groups. The reason may be due to the poor thermal stability and low retention of lutein and zeaxanthin at high temperatures (Llave et al., 2018). Sufficient contact between oil, egg liquid, and steam caused accelerated thermal solidification of the egg liquid, and part of the lutein and zeaxanthin were released with the heat, resulting in a reduction of the final content, and affecting the final yellowness value of the eggs, which is consistent with the conclusion of the previous article (Llave et al., 2018).

The overall color difference between LSG and MLSG and CG is small, all minor. The overall color difference between MHSG and HSG and CG is more than 3, which is a significant difference. Also, under high-temperature and high-speed conditions, the different degrees of mixing of the egg and oil can lead to loss of pigment, which in turn affects the color (Table 4).

3.5. Analysis of texture in scrambled eggs

Texture is one of the most important indicators of food quality and increases consumer satisfaction (Andersen et al., 2019). The difference in Resilience between CG and other groups of scrambled eggs was not significant ($p > 0.05$), but in terms of elasticity the LSG, MLSG, MHSG, and HSG had significantly higher elasticity than CG ($p < 0.05$) (Fig. 5D). The reason is that proteins are denatured at high temperatures and soluble aggregates of high molecular mass are formed through folding. Under the action of disulfide bonds, the proteins are aggregated into a dense mesh structure and eventually form a gel (Li et al., 2018; Liu et al., 2020), which increases the elasticity of the scrambled eggs.

Cohesiveness is the attraction between internal particles that allows

Table 5
Comparison of sensory quality of scrambled egg between control group and experiment groups.

Group	Sensory evaluation index					
	Color (10)	Maturity uniformity (10)	Chewing Flavor (10)	Elastic Hardness (10)	Taste (10)	Overall acceptability (10)
CG	Golden color 8.5[a]	nonuniform overcooked 6.5[a]	Strong egg fragrance 8.8[a]	Weak elasticity, slightly hard 7.5[a]	No roughness 8.0[a]	8.2[a]
LSG	Golden color 8.3[a]	Uniform 8.4[bc]	Strong egg fragrance 8.4[a]	Good elasticity, slightly hard 8.2[b]	Smoothness 8.2[a]	8.4[a]
MLSG	Bright yellow 8.2[a]	Uniform 8.3[bc]	Strong egg fragrance 8.3[a]	Good elasticity, soft and smooth 8.1[b]	Smoothness 7.8[ab]	8.5[a]
MHSG	White yellow 7.8[ab]	Uniform 8.2[b]	Good egg fragrance 7.8[ab]	Good elasticity, soft and smooth 8.4[b]	No roughness 7.7a[b]	7.9[ab]
HSG	White yellow 7.9[b]	Uniform 8.1[b]	Good egg fragrance 7.2[c]	Good elasticity, soft and smooth 8.3[b]	No roughness 7.8[ab]	7.8[ab]

Note: Different letters in the same column indicate significant differences between control group and experiment group ($p < 0.05$).

substances to maintain a certain shape and structural properties. There was a significant difference in the Cohesiveness between MHSG and LSG or MLSG groups ($p < 0.05$) (Fig. 5E). This could be due to the increased steam flow rate and faster evaporation of water molecules from the egg liquid, which affects the protein molecular structure and forms a highly cohesive molecular network (Singh and Ramaswamy, 2013). Steam heating with a high flow rate can provide faster heat transfer, which leads to the rapid evaporation of excess water, enabling the protein molecules to reach the solidification temperature in a shorter time, thus accelerating the solidification process. Moreover, the overall compactness and cohesiveness of scrambled eggs will be enhanced due to the reduction of moisture and the strengthening of protein network structure. In terms of Gumminess, MHSG and HSG were significantly increased than LSG and MLSG ($p < 0.05$) (Fig. 5E). Due to the different steam flow rates, the eggs ripened at different times, resulting in different water content of the samples, which caused changes in the viscosity of the scrambled eggs, consistent with the result in the literature (Shahbaz et al., 2018).

In terms of Hardness, LSG, MLSG, and MHSG differed significantly from the CG ($p < 0.05$) (Fig. 5F). The Hardness of the samples is reduced by the dissociation or hydrolysis of denatured aggregated proteins that occurs when the scramble time is too long (Shahbaz et al., 2018). In addition, the hardness value of HSG was significantly increased, which was related to the extra aggregation of protein structures at high temperatures, producing a stronger spatial structure (Luo et al., 2024; Xue et al., 2020). In terms of Chewiness, MHSG and HSG were significantly increased compared to LSG and MLSG ($p > 0.05$) (Fig. 5F). The steam ripening process increases the degree of denaturation and gelatinization of proteins(Juliano et al., 2012), which affects the chewability of eggs (Singh and Ramaswamy, 2013).

3.6. Analysis of sensory quality in scrambled eggs

The organoleptic scores of Colors, Chewing Flavor, and Taste of CG did not differ significantly from the results of LSG and MLSG ($p > 0.05$), and all the above three groups were better than MHSG and HSG. The Elastic hardness score and Maturity uniformity of the CG differed significantly from the other groups ($p < 0.05$), indicating that the scrambled eggs by the automatic scrambler had low elasticity and a slightly hard texture. The samples in the CG were over-ripened or unevenly ripened in some areas due to the uneven distribution of the heat field in the pot and insufficient enthalpy exchange. However, the use of steam heating has better thermal convection uniformity. Regarding Overall acceptability, all groups had an overall smooth texture with no roughness (Table 5).

4. Conclusion

To solve the problem of defective existing industrialized scrambled egg devices, this paper demonstrates high-throughput continuous steam scrambled egg devices and verifies their production performance. The device can precisely adjust the steam flow to achieve different shapes of egg pieces satisfying diversified processing needs and has about 5 times the capacity of an automatic scrambler, suitable for large-scale industrial dishes production needs and expanding product lines and markets (e.g. fast-food chains, central kitchens, etc). The heat transfer process between steam and egg liquid is simulated by CFD to investigate the effect of different steam flow rates on the state of the egg liquid and the trajectory of the egg liquid after entering the pipeline. Performance Verification results are consistent with previously derived relationships between egg block shape and steam flow rate as well as CFD simulations. Most importantly, steam heating technology provides even heat distribution to ensure that the egg liquid solidifies evenly in a short time, avoiding overcooking or undercooking and maintaining the consistency and taste of the food. The results of performance validation showed that the finished scrambled egg of this device has good overall elasticity and was soft, which has better maturity uniformity and is acceptable to consumers.

In summary, this steam scrambled egg device provides technical support for the industrial production of prepared dishes and specialized cooking equipment.

Credit author statement

Liangyu Xue: Investigation, Writing- Original draft preparation. Xiaojia Hu: Experimental design, Software.Wensong Wei: Experimental design, Data interpretation, Writing - review.Ping Yang, Xin Ai: Methodology, Funding acquisition.Bo Qi, Yibing Yuan, Fangting Fu: Project management.Chunhui Zhang: Funding acquisition, Supervision.

Declaration of competing interest

The authors declare that they have no known competing financial interests or personal relationships that could have appeared to influence the work reported in this paper.

Acknowledgments

This work was supported by the 14th Five-Year National Key Research and Development (2023YFD2100700), National Science Fund for Distinguished Young Scholars (32201952), the Agricultural Science and Technology Innovation Program of Institute of Food Science and Technology, Chinese Academy of Agricultural Sciences (CAAS-ASTIP-G2022-IFST-08), and Chinese Academy of Agricultural Sciences (CAAS) Digital Agricultural and Rural Research Institute (Zibo) Innovation Team Funding.

Appendix A. Supplementary data

Supplementary data to this article can be found online at https://doi.

org/10.1016/j.crfs.2024.100948.

Data availability

Data will be made available on request.

References

Adler-Nissen, J., 2007. Continuous wok-frying of vegetables: process parameters influencing scale up and product quality. J. Food Eng. 83 (1), 54–60. https://doi.org/10.1016/j.jfoodeng.2006.11.002.

Andersen, B.V., Brockhoff, P.B., Hyldig, G., 2019. The importance of liking of appearance, -odour, -taste and -texture in the evaluation of overall liking. A comparison with the evaluation of sensory satisfaction. Food Qual. Prefer. 71, 228–232. https://doi.org/10.1016/j.foodqual.2018.07.005.

Bohr, T., Scheichl, B., 2021. Surface tension and energy conservation in a moving fluid. Physical Review Fluids 6 (5), L052001. https://doi.org/10.1103/PhysRevFluids.6.L052001.

Chapin, R.A., 1983. Method and Apparatus for Automated Chinese Stir-Fry Cooking. US.

Chen, F., Zhang, M., Yang, C.-h., 2020. Application of ultrasound technology in processing of ready-to-eat fresh food: a review. Ultrason. Sonochem. 63, 104953. https://doi.org/10.1016/j.ultsonch.2019.104953.

Coimbra, J.S.R., Gabas, A.L., Minim, L.A., Garcia Rojas, E.E., Telis, V.R.N., Telis-Romero, J., 2006. Density, heat capacity and thermal conductivity of liquid egg products. J. Food Eng. 74 (2), 186–190. https://doi.org/10.1016/j.jfoodeng.2005.01.043.

Dansou, D.M., Zhang, H., Yu, Y., Wang, H., Tang, C., Zhao, Q., Qin, Y., Zhang, J., 2023. Carotenoid enrichment in eggs: from biochemistry perspective. Animal Nutrition 14, 315–333. https://doi.org/10.1016/j.aninu.2023.05.012.

Fryer, P.J., Robbins, P.T., 2005. Heat transfer in food processing: ensuring product quality and safety. Appl. Therm. Eng. 25 (16), 2499–2510. https://doi.org/10.1016/j.applthermaleng.2004.11.021.

Harding, K.G., 2018. Heat Transfer Introduction.

Hoznedl, M., Gregor, K.B.M., 2020. Numerical and Analytical calculation of flow during steam blowing. MATEC Web of Conferences.

Jia, Y., Hu, L., Liu, R., Yang, W., Khalifa, I., Bi, J., Li, Y., Zhen, J., Wang, B., Zhang, Z., Zhang, E., Li, B., 2024. Innovations and challenges in the production of prepared dishes based on central kitchen engineering: a review and future perspectives. Innovat. Food Sci. Emerg. Technol. 91, 103521. https://doi.org/10.1016/j.ifset.2023.103521.

Juliano, P., Bilbao-Sáinz, C., Koutchma, T., Balasubramaniam, V.M., Clark, S., Stewart, C. M., Dunne, C.P., Barbosa-Cánovas, G.V., 2012. Shelf-stable egg-based products processed by high pressure thermal Sterilization. Food Eng. Rev. 4 (1), 55–67. https://doi.org/10.1007/s12393-011-9046-4.

Lee, A.P., Barbano, D.M., Drake, M.A., 2017. The influence of ultra-pasteurization by indirect heating versus direct steam injection on skim and 2% fat milks. J. Dairy Sci. 100 (3), 1688–1701. https://doi.org/10.3168/jds.2016-11899.

Li, J., Deng, Y., Xu, W., Zhao, R., Chen, T., Wang, M., Xu, E., Zhou, J., Wang, W., Liu, D., 2023. Multiscale modeling of food thermal processing for insight, comprehension, and utilization of heat and mass transfer: a state-of-the-art review. Trends Food Sci. Technol. 131, 31–45. https://doi.org/10.1016/j.tifs.2022.11.018.

Li, J., Li, X., Wang, C., Zhang, M., Xu, Y., Zhou, B., Su, Y., Yang, Y., 2018. Characteristics of gelling and water holding properties of hen egg white/yolk gel with NaCl addition. Food Hydrocolloids 77, 887–893. https://doi.org/10.1016/j.foodhyd.2017.11.034.

Li, J., Wang, C., Gu, L., Su, Y., Chang, C., Yang, Y., 2020. Gel properties of salty liquid whole egg as affected by preheat treatment. J. Food Sci. Technol. 57 (3), 877–885. https://doi.org/10.1007/s13197-019-04119-4.

Lian, M., He, K., Ratkowsky, D.A., Chen, L., Wang, J., Wang, L., Yao, W., Shi, P., 2024. Comparison of egg-shape equations using relative curvature measures of nonlinearity. Poultry Sci. 103 (10), 104069. https://doi.org/10.1016/j.psj.2024.104069.

Liu, X., Wang, J., Huang, Q., Cheng, L., Gan, R., Liu, L., Wu, D., Li, H., Peng, L., Geng, F., 2020. Underlying mechanism for the differences in heat-induced gel properties between thick egg whites and thin egg whites: gel properties, structure and quantitative proteome analysis. Food Hydrocolloids 106, 105873. https://doi.org/10.1016/j.foodhyd.2020.105873.

Llave, Y., Fukuda, S., Fukuoka, M., Shibata-Ishiwatari, N., Sakai, N., 2018. Analysis of color changes in chicken egg yolks and whites based on degree of thermal protein denaturation during ohmic heating and water bath treatment. J. Food Eng. 222, 151–161. https://doi.org/10.1016/j.jfoodeng.2017.11.024.

Luo, X., Tan, J.e., Yao, Y., Wu, N., Chen, S., Xu, L., Zhao, Y., Tu, Y., 2024. Effects of different temperatures on the physicochemical characteristics, microstructure and protein structure of preserved egg yolk. Food Chem. X 22, 101278. https://doi.org/10.1016/j.fochx.2024.101278.

Mead-Hunter, R., King, A.J.C., Mullins, B.J., 2012. Plateau Rayleigh instability simulation. Langmuir 28 (17), 6731–6735. https://doi.org/10.1021/la300622h.

Safavi Nic, S.S., Buist, K.A., Verdurmen, R.E.M., Kuipers, J.A.M., 2020. Dynamic model to predict heat-induced protein denaturation and fouling in a Direct Contact Steam Condensation process. Chem. Eng. Sci. X 8, 100075. https://doi.org/10.1016/j.cesx.2020.100075.

Sâmia, R.R., Lorenzo, N.D., Lessa Barbosa, B.V., Ferreira Fonseca, A.L., Nunes, C.A., Bastos, S.C., 2022. Lipid quality of fried and scrambled eggs prepared in different frying medium. Int. J. Gastron. Food Sci. 29, 100552. https://doi.org/10.1016/j.ijgfs.2022.100552.

Sangsom, W., Inprasit, C., 2022. Design and development of Innovative steam injection for high-temperature short-time liquid foods. Processes 10 (1), 161.

Shahbaz, H.M., Jeong, B., Kim, J.U., Ha, N., Lee, H., Ha, S.-D., Park, J., 2018. Application of high pressure processing for prevention of greenish-gray yolks and improvement of safety and shelf-life of hard-cooked peeled eggs. Innovat. Food Sci. Emerg. Technol. 45, 10–17. https://doi.org/10.1016/j.ifset.2017.09.016.

Singh, A., Ramaswamy, H.S., 2013. Effect of high pressure processing on color and textural properties of eggs. J. Field Robot. 2, 11–24.

Subramanian, R.S., 2014. Heat Transfer in Flow through Conduits.

Wang, Q., Yang, Y., Li, Z., Jin, H., Shu, D., Jin, Y., Jin, G., Sheng, L., 2024. Research advances on the effects of thermal and non-thermal processing techniques on the physicochemical properties and microbiological control of liquid eggs. Food Control 155, 110106. https://doi.org/10.1016/j.foodcont.2023.110106.

Wang, X., Zhao, Z., 2023. A mini-review about direct steam heating and its application in dairy and plant protein processing. Food Chem. 408, 135233. https://doi.org/10.1016/j.foodchem.2022.135233.

Xue, H., Tu, Y., Xu, M., Liao, M., Luo, W., Guo, W., Zhang, G., Zhao, Y., 2020. Changes in physicochemical properties, gel structure and in vitro digestion of marinated egg white gel during braising. Food Chem. 330, 127321. https://doi.org/10.1016/j.foodchem.2020.127321.

Zhao, Y., Yue, S., Zhang, Y., Wang, H., 2023. Flow velocity computation using a single ERT sensor. Flow Meas. Instrum. 93, 102433. https://doi.org/10.1016/j.flowmeasinst.2023.102433.